Polymer 51 (2010) 1744–1751

Contents lists available at ScienceDirect

Polymer

journal homepage: www.elsevier.com/locate/polymer

In situ evaluation of structural changes in poly(ester-urethanes) during shape-memory cycles

I.M. Pereira [a], R.L. Oréfice [b,*]

[a] Federal Center of Technological Education of Minas Gerais, Timoteo, Brazil
[b] Federal University of Minas Gerais, Department of Metallurgical and Materials Engineering, Belo Horizonte, Brazil

ARTICLE INFO

Article history:
Received 4 January 2010
Received in revised form
19 February 2010
Accepted 21 February 2010
Available online 1 March 2010

Keywords:
Shape memory properties
SAXS
Poly(ester-urethane)

ABSTRACT

The relationship between shape-memory behavior and structure was studied using three series of poly (ester-urethanes) with varying amounts of hard segment. The materials were designed to display a three-phase structure consisting of a disperse phase of crystallites and hard domains embedded in an amorphous matrix based on soft segment. Structure and thermal properties of the resultant materials were investigated using techniques such as modulated differential scanning calorimetry (MDSC), dynamic mechanical analysis (DMA) and small angle X-ray scattering (SAXS). The results revealed morphological changes in the materials during a low temperature shape-memory cycle. To study shape recovery, a deformed specimen was evaluated on a heating stage mounted at the SAXS beamline. Furthermore, to study the effect of temperature during recovery, the specimens were subjected to different thermo-cycles. Under each set of conditions, the phase morphology and composition were investigated. Temporary shape was stored by the metastable structure formed during deformation. The recovery was triggered by the melting of crystallites and hydrogen bonding between hard domains. The recovery process was divided into three stages. Bulk incompatibility and entropic recovery determined the final polyurethane morphology.

1. Introduction

Linear segmented thermoplastic polyurethane (PU) elastomers are multiblock copolymers consisting of hard and soft segments that can separate to form hard and soft domains. The properties of these materials are dependent on phase morphology and the separation of hard and soft domains [1–3]. Recent methods have tailored the properties of PU to yield thermo-responsive materials that can be used to create smart devices capable of memorizing a permanent shape that is substantially different from the initial temporary shape [4]. These materials have been referred to as shape-memory polymers (SMP). In SMPs, the relative motion and rearrangement of molecular chains is the primary inelastic strain mechanism responsible for the shape-memory effect. The establishment and annihilation of a metastable structure allows for the storage of temporary shape and recovery from deformation during an SM cycle. For instance, to store a deformed shape in a stable manner, new chain positions must be fixed by new bonds (physical or chemical bonds). A fixed shape can be achieved by cooling the material below the transition temperature after significant chain alignment and chain slip occur. The newly formed bonds provide a storage mechanism for macroscopic stress and increased chain organization (lower entropy). To recover the original shape, the material is heated and temporary bonds are subsequently broken. At higher temperatures, the bonds are weakened and the low entropy state drives individual chains back to their original position, facilitating shape recovery [5,6].

With the use of small-angle X-ray scattering, the objective of this study was to monitor morphology development during shape-memory thermomechanical cycles of polyurethanes with different amounts of hard segments and to describe the relationship between morphology evolution and observed shape-memory properties.

2. Materials and methods

2.1. Polymer synthesis

Poly(caprolactone diol) (PCL – Mn = 1250, 2000 g mol^{-1}), isophorone diisocyanate (IPDI), 2,2-bis(hydroxymethyl), propionic acid (DMPA) and dibutyl tin dilaurate (DBDLT) were obtained from Aldrich (St. Louis, MO). Triethylamine (TEA, 98%) and hydrazine

* Corresponding author. Tel.: +55 31 3409 1843; fax: +55 31 3409 1815.
E-mail address: rorefice@demet.ufmg.br (R.L. Oréfice).

0032-3861/$ – see front matter © 2010 Elsevier Ltd. All rights reserved.
doi:10.1016/j.polymer.2010.02.037

Table 1
Composition (wt.%) of waterborne PUs.

	PCL		DMPA	IPDI	HZ	TEA	W(HS)
	1250	2000					
PU-I	55.4	–	4.5	34.6	2.1	3.4	38.0
PU-II	23.7	37.9	3.8	29.6	2.1	2.9	32.6
PU-III	–	66.1	3.3	25.8	1.9	3.0	28.5

(HZ, 25%) were purchased from Vetec (RJ, Brazil). All chemicals employed in this study were used without prior treatment.

PUs were prepared according to the prepolymer mixing method. PCL and DMPA were stirred in a glass reactor at 65 °C for 30 min. IPDI was added to the reactor in the presence of DBDLT (NCO/OH ratio of 2) under a N_2 atmosphere. The reaction was carried out at 70–75 °C for 3 h. The prepolymer and carboxylic acid groups were neutralized by the addition of TEA. Water dispersion and PU chain extension were achieved by adding HZ and deionized water to the neutralized prepolymer under high-speed stirring. This synthesis is described in previous work [7]. The feed ratios are indicated in Table 1, where W(HS) is weight fraction of the hard segment obtained from Equation (1).

$$W(HS) = \frac{Weight_{IPDI} + Weight_{HZ}}{Weight_{PU}} \times 100 \quad (1)$$

2.2. Modulated differential scanning calorimetry (MDSC)

MDSC experiments were performed using a TA Instruments 2920. The following protocol was applied to each sample: (1) the sample was heated from room temperature to 110 °C at a rate of 15 °C min^{-1}, (2) held for 3.00 min at 110 °C, (3) cooled to −110 °C at 3.00 °C/min, modulating +/− 1.00 °C every 60 s, (4) held for 3.00 min at −110 °C and (5) heated again to 110 °C at a rate of 3.00 °C/min, modulating +/− 1.00 °C every 60 s. The melting temperature was determined as the peak maxima in DSC curve and the glass transition temperature (T_g) was established as the mid-point between baseline changes by calorimeter software.

2.3. Dynamic mechanical analysis (DMA)

Dynamic mechanical properties were investigated by a TA Instruments DMA 800 with a single cantilever clamp at a heating rate of 3 °C/min under an N_2 atmosphere. The test frequency was 5 Hz and the temperature varied from −100 °C to 90 °C.

2.4. Mechanical properties

The tensile strength (σ_m), elongation at break (ε_m), Young's modulus (E), toughness and resilience of the samples (DIN60) were measured using a universal testing machine (DL3000, EMIC) at a strain rate of 0.5 min^{-1}. The tests were performed at 28 °C (room temperature). Toughness and resilience, which represent the energy absorbed until rupture and the energy absorbed during elastic deformation, respectively, were obtained by integrating the stress-strain curves. Scheme 1 illustrates the method for determining values of toughness and resilience.

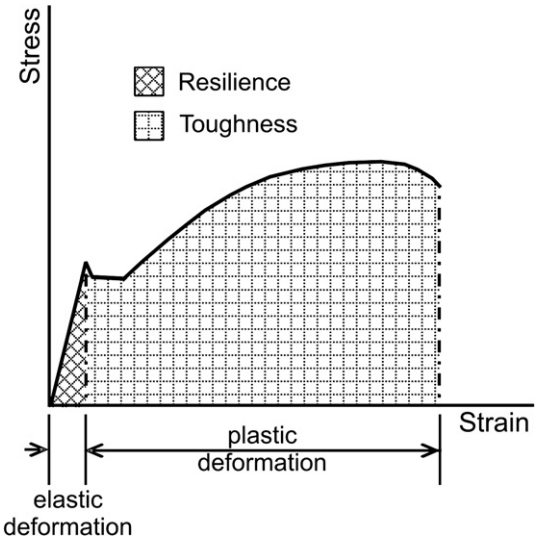

Scheme 1. Determination of toughness and resilience from stress-strain curves.

2.5. Shape-memory properties (SM)

SM experiments were conducted at room temperature using a universal testing machine (DL3000, EMIC), where the sample length between clamps was 20 mm. The shape recovery cycle consisted of the following steps: (1) The samples (DIN60) were deformed to approximately L_m = 120 mm at a crosshead speed of 10 mm/min (2) While maintaining the strain at L_m, the samples were removed from the grips and cooled with liquid N_2. (3)The mechanical constraints on the polymers were removed at room temperature. (4) The samples were subsequently heated in an oven and maintained at this temperature to recover their original shape.

To study the effect of step 4 of the SM cycle on shape recovery, PU-III samples were submitted to different thermo-cycles and allowed to recover their original shape. In cycle-A, the deformed sample was heated to 37 °C in an oven and maintained at this temperature for 17 h. Recovery during thermo-cycle "B" was conducted in two heating stages: the specimen was initially heated to 37 °C for 17 h and subsequently heated for 10 min at 50 °C. In thermo-cycle "C", the sample was heated to 50 °C for 30 min. Finally, in cycle-E, the sample was maintained at 80 °C for 20 min. PU-I and PU-II were submitted exclusively to cycle-E to recover

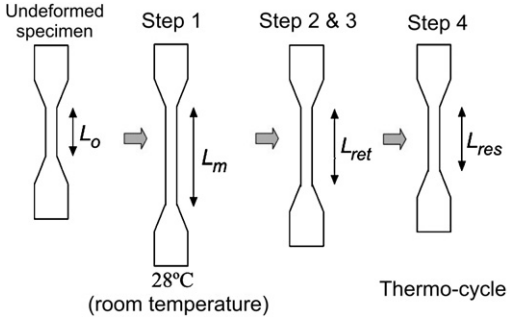

	Temperature	time
Cycle-A	37ºC	17 hs
Cycle-B	37ºC	17 hs
	50ºC	10 min
Cycle-C	50ºC	30 min
Cycle-E	80ºC	20 min

Fig. 1. Steps in the SM cycle and thermo-cycle parameters.

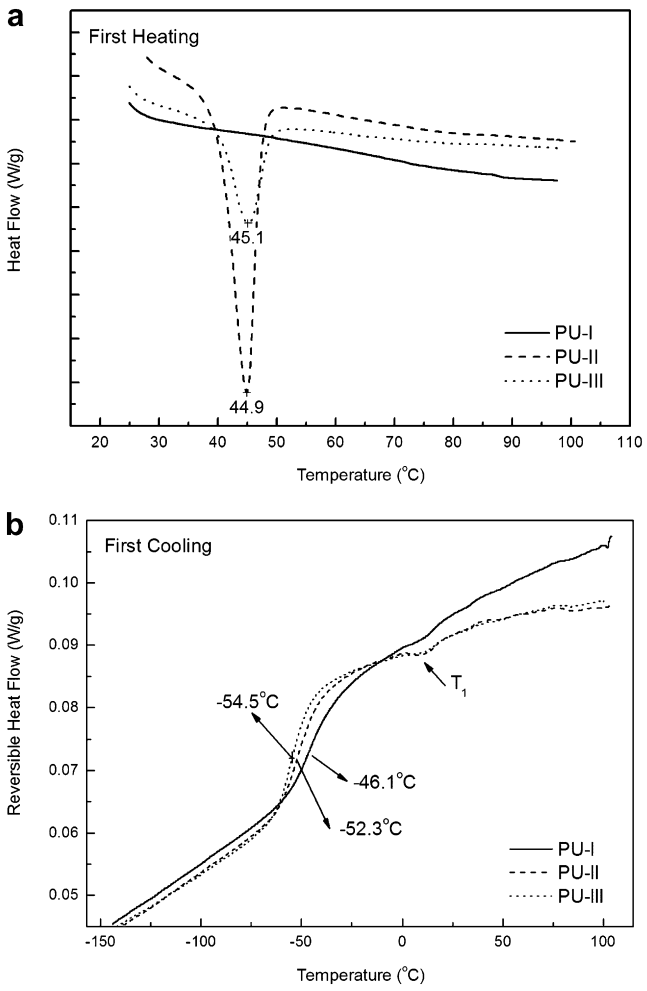

Fig. 2. DSC curves of the obtained PUs: (a) initial heating (b) initial cooling.

their original shape. Fig. 1 describes the steps of the SM cycle and thermo-cycle parameters.

SM properties of the materials were described by the strain recovery ratio, R_R, and the strain fixity ratio, R_f. These parameters were determined according to Equations (2) and (3), respectively:

$$R_r(\%) = \frac{L_m - L_{Res}}{L_m - L_o} \times 100 \quad (2)$$

$$R_f(\%) = \frac{L_{Ret} - L_o}{L_m - L_o} \times 100 \quad (3)$$

where L_o is the original length, L_m is the deformed length, L_{ret} is retained length and L_{res} is the length after recovery.

Table 2
DSC results of PUs.

	T_g (°C)	T_{onset} (°C)	T_{end} (°C)	Zone width	T_1 (°C)	T_m (°C)
PU–I	−46.1	−53.8	−33.6	20.2	19.0	–
PU–II	−52.3	−58.2	−42.4	15.8	21.9	44.9
PU–III	−54.5	−59.6	−46.4	13.2	15.4	45.1

T_g = Glass transition temperature.
T_{onset} = Onset of glass transition.
T_{end} = End of glass transition.
Zone width = $T_{end}-T_{onset}$.
T_1 = Endothermic inflection point associated with clusters of short, hard segments.
T_m = Melting temperature.

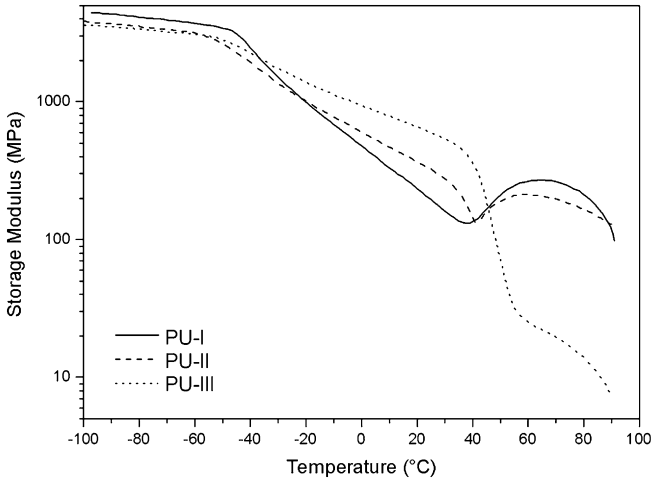

Fig. 3. DMA storage modulus as a function of temperature.

2.6. Synchrotron small angle X-ray scattering (SAXS)

SAXS measurements of synchrotron small angle X-ray scattering were performed using the beamline of the National Synchrotron Light Laboratory (LNLS, Campinas, Brazil). After passing through a thin beryllium window, the beam was monochromatized (λ = 1.488 Å) and horizontally focused by a cylindrically bent and asymmetrically cut silicon single crystal. The X-ray scattering intensity, $I_{(q)}$, was experimentally determined as a function of the scattering vector, q, which was obtained according to Equation (4):

$$q = \frac{4\pi}{\lambda}\sin\theta \quad (4)$$

where λ is the X-ray wavelength and θ is half the scattering angle.

Each SAXS pattern corresponded to a data collection period of 900 s. Parasitic scattering intensity produced by the collimating slits was subtracted from the experimental scattering intensity produced by the samples. All SAXS patterns were corrected for non-constant sensitivity of the position-sensitive X-ray detector, intensity of the direct synchrotron beam and for differences in sample thickness. Due to the normalization procedure, the SAXS intensity was determined for all samples in the same arbitrary units, allowing a direct comparison to be made between samples. A sample-detector distance of 551.6 mm was used during the measurements.

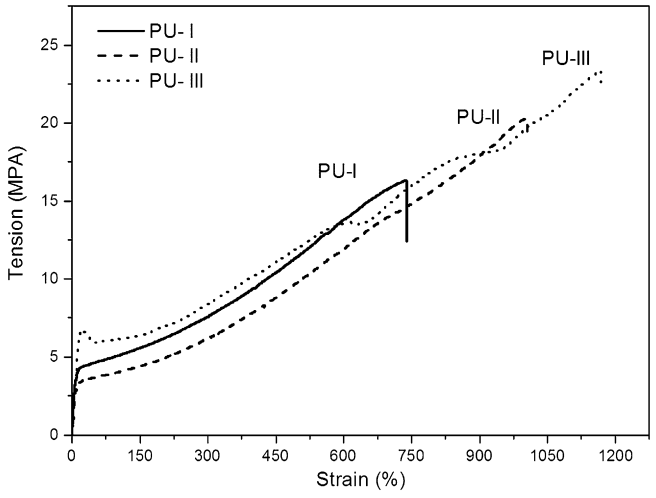

Fig. 4. Stress-strain curves of PUs.

Table 3
Mechanical and SM properties of PU–I, PU–II and P–III (average of 4 measurements).

PU	σ_m (MPa)	ε_m (%)	E (MPa)	Resilience (MJ/m^3)	Toughness (MJ/m^3)	R_f (%)	R_R (%)			
							Cycle-A	Cycle-B	Cycle-C	Cycle-E
I	16.5 ± 0.4	768 ± 61	3.3 ± 0.6	5.6 ± 0.2	1467 ± 176	14 ± 0.8	N.A	N.A	N.A	92.9 ± 0.3
II	20.7 ± 2	1053 ± 45	2.4 ± 0.4	5.9 ± 0.8	2288 ± 270	20 ± 0.5	N.A	N.A	N.A	94.0 ± 0.1
III	22.5 ± 2	1211 ± 41	2.1 ± 0.6	7.8 ± 2.7	2831 ± 337	31 ± 2.2	71	82	88	98.2 ± 0.8

σ_m = Tensile strength.
ε_m = Elongation at break.
E = Young modulus.
R_f = Strain fixity ratio.
R_R = Strain recovery ratio.
N.A. = not available.

2.7. *In situ* recovery

A deformed PU-III specimen was placed on a heating stage mounted at the beamline. The specimen was heated to 50–60 °C and shape recovery was measured over 20 min. SAXS patterns were recorded at 7.2 min, 8.3 min, 9.3 min, 11.0 min, 12.1 min, 13.1 min, 14.2 min, 15.2 min, 16.3 min, 17.3 min, 18.4 min and 19.4 min.

3. Results

In DSC analysis, the width of the transition zone provides a qualitative measure of phase homogeneity and the variation in T_g indicates the degree of miscibility. Thus, the amount of hard segments dissolved in soft domains can be studied by monitoring T_g of soft domains [8]. In the first run, shown in Fig. 2(a) a first order transition around 45 °C was observed for PU–II and PU–III, corresponding to the melting of PCL-rich crystals. Neither the endothermic melting peak associated with the crystalline fraction, nor a crystallization peak was observed for samples during the second heating run or in the cooling run, respectively. This result may be due to the fast heating/cooling rates employed during subsequent DSC runs. As shown in Fig. 2(b), a glass transition around −60 ° C was observed in the cooling run. A shift of T_g to higher temperatures indicated a higher concentration of dissolved hard segments. According to DSC results, the degree of phase miscibility of PUs displayed the following trend: PU–I > PU–II > PU–III. Thus, PUs with higher concentrations of hard segments displayed soft domains rich in hard segments.

All PUs displayed a small endothermic inflection centered at T_1, associated with hard segment domains. According to Seymour and Cooper [9], the endotherm observed in DSC may be attributed to a morphological effect that is a function of hard segment length. Clusters of short hard segments yield lower temperature endotherms [8,9]. Thermal properties are summarized in Table 2.

The storage modulus, E', of the PUs is shown in Fig. 3. Two significant declines in E' were observed for all samples during heating, ascribed to glass and melting transitions of the soft segment phase. Below the glass transition temperature, the glass state modulus increased with increasing hard segment content. This is due to a larger phase and a resultant increase in the number of strong interactions among amorphous hard domains in the glass state. A higher glass modulus is desired in an SM material because a larger shape fixity occurs upon cooling [10]. Above the melting transition, the storage modulus of PU-III decreased with increasing temperature. However, storage moduli of PU–I and PU–II increased. Above the soft-segment melting point, the storage modulus was strongly dependent on hydrogen bonding between hard segments. Highly hydrogen bonded hard segments of PU–I and PU–II generated a reinforcing effect which contributed to the enhancement of the rubbery modulus plateau [11–13], causing the v-shape observed in Fig. 3. Thus, at a temperature above the melting point, the storage modulus is controlled by the number of hard segments present in the polymer. At a temperature between T_g and the melting point of soft segments, a partially crystalline state of soft domains and interactions between amorphous hard domains in a rubbery state yields a high storage modulus, as observed in PU-III [13].

Fig. 4 shows the stress-strain curves of PUs used in the investigation. Table 3 summarizes the mechanical and SM properties of each PU, where data points are an average of four measurements. The results indicated that an increase in W(HS) produced a decrease in strain and stress at rupture, and an increase in modulus. These results show that the mechanical properties of PUs are highly dependent on the hard segment content, which concurs with previous reports [14–16]. Hard segments can associate via hydrogen bonds which leads to an enhancement in stiffness. However, hydrogen bonding also prevents chain slippage. As shown in Table 3, upon removing the mechanical constraints in step 3, low strain fixity ratios were observed for all PUs. Moreover, thermo-cycle "E" promoted more than 90% shape recovery for hard segments. Thus, the results indicated that the thermo-cycle configuration has a stronger effect on R_R than W(HS).

Scheme 2 is a schematic of the thermomechanical cycle employed in this study. Fig. 5 illustrates SAXS patterns of PUs during different stages of the SM thermomechanical cycle, and during *in situ* recovery. The SAXS measures scattering intensity as a function of the

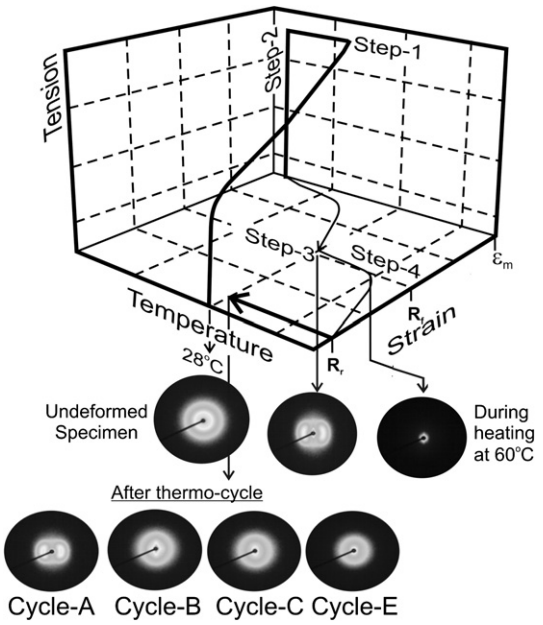

Scheme 2. Schematic representation of the thermomechanical cycle employed during the investigation.

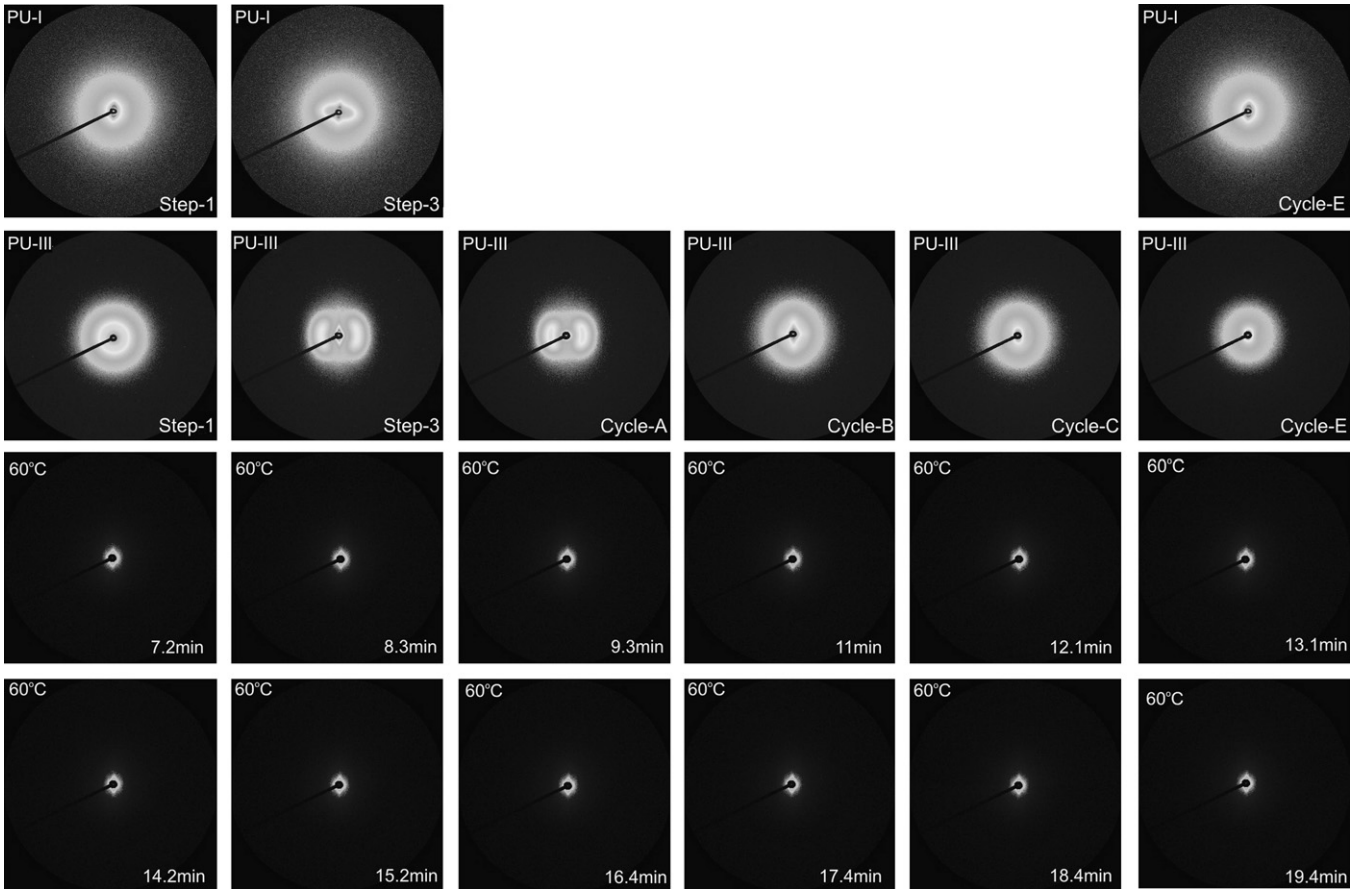

Fig. 5. SAXS 2D patterns for PUs during different stages of the SM thermomechanical cycle and *in situ* recovery.

incident X-ray beam and yields information on morphology at the nanometer level because it is sensitive to differences in electron density within a material. The patterns and intensity distribution of SAXS are also dependent on the shape, size and distribution of scattering objects [17]. In Fig. 4, two maxima oriented along the direction of stretching were observed in step 3 on both sides of the beam stopper. These maxima are due to scattering from an oriented structure that formed during deformation. SAXS patterns also indicated that a high degree of orientation was obtained during deformation [18]. The thermo-cycles applied during recovery led to different amounts of reorientation in the deformed structure. SAXS patterns are a function of energy infused into the system during the thermo-cycle: higher temperature treatments introduced more energy into the system, and yielded SAXS patterns that were similar to those of the original materials prior to deformation, which indicated that the initial morphology was restored.

Fig. 6(a) illustrates SAXS data derived from the integration of 2-D patterns exhibited in Fig. 4 during different stages of the SM thermomechanical cycle. The observed scattering peak is due to local heterogeneities in electron density of materials and is usually interpreted as a consequence of distinct microphases with different electron densities. In Fig. 6(b), the Lorentz correction (a plot of q

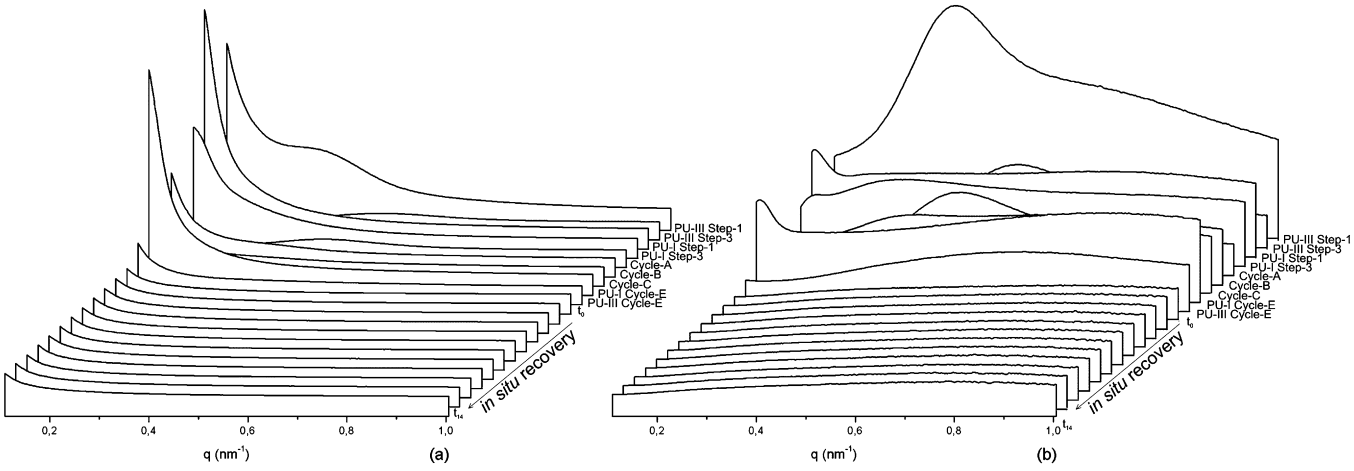

Fig. 6. (a) Original SAXS data and (b) Lorentz corrected SAXS patterns for PUs during different stages of the SM thermomechanical cycle and *in situ* recovery.

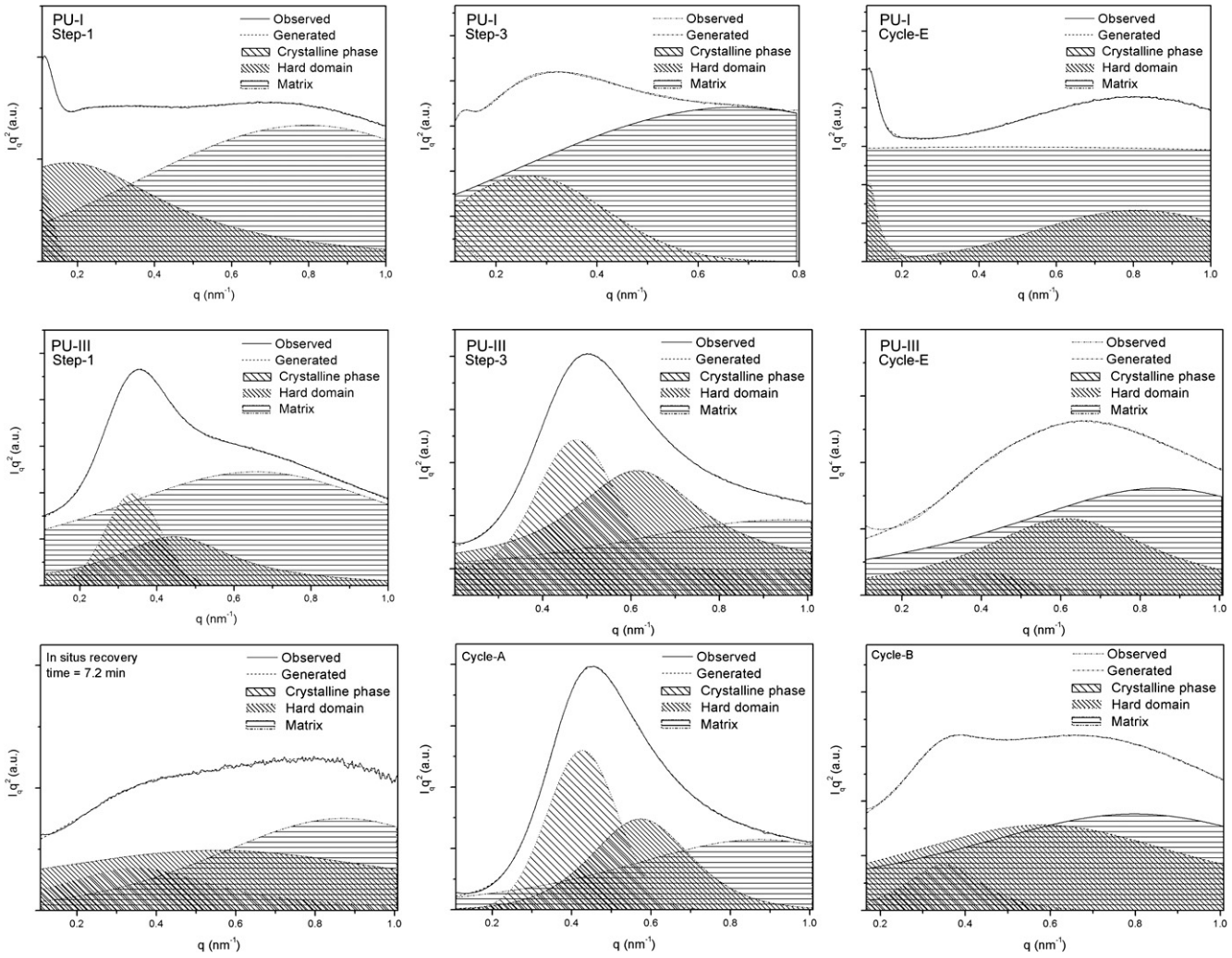

Fig. 7. Deconvoluted Lorentz SAXS pattern of PU-I and PU-III during different steps of the SM cycle.

versus $I_{(q)}q^2$) was applied to SAXS data to emphasize small scattering peaks. Moreover, to provide information on the overall difference in electron density of the samples, the invariant Q was calculated by integrating the curve generated by the Lorentz correction (Equation (5)) [17,19,20]. High values of Q_{inv} are typically associated with nanostructures formed by phase separation [17,19,20].

$$Q_{inv} = \int_0^\infty I_{(q)}q^2 dq \tag{5}$$

PUs were composed of three-phases including an amorphous matrix (soft segment), hard domains and crystalline segments. The contribution of each phase to the Lorentz corrected SAXS patterns were separated according to a deconvolution procedure. Fig. 7 illustrates deconvoluted SAXS data during different stages of the SM thermomechanical cycle. Q_{inv} of each phase was obtained as a fraction of the total area. The deconvoluted crystalline phase was associated with higher integrated values and higher electronic density [21]. As shown in Table 4, the ratio of matrix to dispersed

Table 4
Deconvoluted SAXS results.

		Permanent Shape	Step-3	Cycle-A	Cycle-B	Cycle-C	Cycle-E
		Q_{inv} (%)	Q_{inv} (%)	Q_{inv} (%)	Q_{inv} (%)	Q_{inv} (%)	Q_{inv} (%)
PU-I	matrix	66.80	75.35	N.A	N.A	N.A	77.44
	domains	31.48	24.03	N.A	N.A	N.A	19.79
	crystals	1.72	0.62	N.A	N.A	N.A	2.77
PU-III	matrix	68.96	25.65	38.08	48.44	60.50	58.15
	domains	17.50	43.82	28.37	43.66	31.65	35.58
	crystals	13.53	30.52	33.55	7.90	7.85	6.27
Ratio		Initial	Step-3	Cycle-A	Cycle-B	Cycle-C	Cycle-E
Matrix	PU–I	2.01	3.06	N.A	N.A	N.A	3.43
Disperse Phase	PU–III	2.22	0.35	0.61	0.94	1.53	1.38

N.A. = not available.

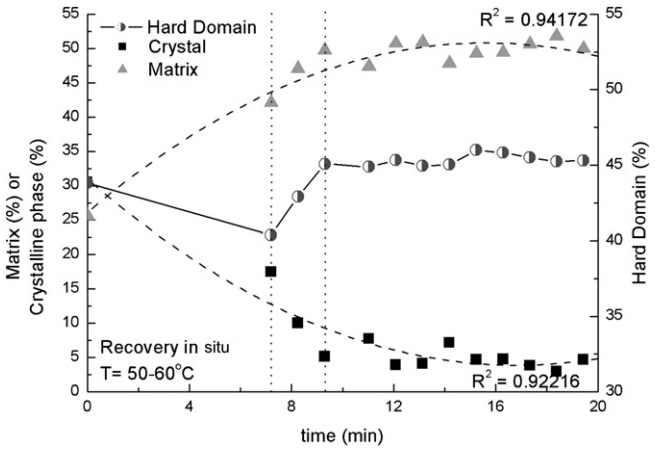

Fig. 8. PU phase evolution during the *in situ* SAXS test.

phase (i.e. crystals and hard domains) indicated an evolution of morphology during the SM cycle.

As observed in Fig. 8, shape recovery during *in situ* SAXS experiments occurred within three stages. In stage 1 of the recovery, the number of hard domains decreased and then rapidly increased in the second stage. Finally, in the third stage, the number of hard domains remained stable.

4. Discussion

When a material is deformed, polymer chains orient along the direction of extension and induce crystallization. According to Table 4, deformation induced changes in the proportion of phases in PU-III, promoting crystallization and phase separation. However, crystallization was not observed in PU–I after step 3 of the SM cycle. Moreover, neither PU–I nor PU-III were efficient in recovering the original ratio of matrix to disperse phase (the disperse phase is formed by hard domains and crystals) after step 4. Nevertheless, PU-III promoted more recovery than PU–I after step 3. The matrix to disperse phase ratio of PU-III increased from 0.35 to 1.38, while PU–I increased from 3.06 to 3.43.

The efficiency of an SM polymer is controlled by the chemical architecture of the polymer, molar mass, degree of cross-linking, and the fraction of amorphous and crystalline domains [22]. In the present study, entanglement, hydrogen bonding and crystallinity were used as tools to force memorization of the PUs original shape. The development of new physical entanglements (temporary bonds) between polymeric chains and the creation of new crystals were used to produce a metastable structure and maintain the deformed shape in a stable manner. As observed in Fig. 5 and Table 4, PU–I is less efficient than PU-III in promoting crystallization during chain slippage. When deformation was applied to PU–I, polymer chains aligned with the direction of extension. However, the high degree of phase mixing in PU–I hindered the formation of new crystals and metastable structure development. Therefore, R_f values of PU–I are less than PU-III. Nevertheless, upon removal of strain at step 3, a significant recovery occurred and low values of R_f were observed. The SM cycle configuration may have contributed to these results. To maintain a deformed shape in a stable manner, new chain positions must be fixed by new bonds. The development of new physical entanglements (temporary bonds) between polymeric chains is a result of temperature reduction and/or forced chain alignment [5]. After step 1, samples were clamped to an apparatus and immersed in liquid nitrogen. As a result, the metastable structure developed during strain was partially released and contributed to low values of R_f . Additionally, recovery temperature may also contribute to R_f values. According to Ping et al. [23], when the deformation temperature is too low (30 °C below the melting temperature of soft segments), shape recovery begins at a lower temperature and occurs over a wide range. Experiments conducted at ambient temperature were typically higher than 25 °C; however, the lowest recovery temperature may have been lower than room temperature and shape recovery may have begun immediately after step 3.

Reversibility was designed to occur during the softening of soft domains or the melting of crystallites. However, shape recovery is also highly dependent on hydrogen bonding. As observed in Fig. 3, strong interactions between hard segments provided sufficient energy to restore the polymer back to its original shape after melting. The values of toughness in Table 3 may be correlated to R_f or R_R. In the present study, crystallization occurred during deformation and prevented the movement of polymeric chains, thereby increasing the energy absorbed during deformation. This mechanism is significant because energy stored in the material allows the system to restore its original structure after being deformed.

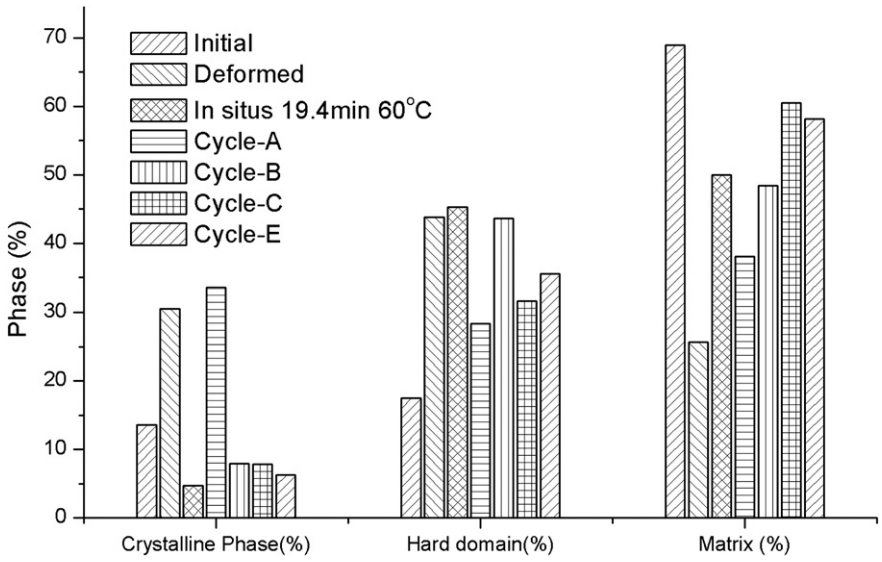

Fig. 9. PU phase evolution during different steps of the SM cycle.

During *in situ* tests, the size of the crystalline fraction decreased because soft segment crystals melted and enriched the matrix phase with soft segments (first stage). As a result, the balance between hard and soft segments in the bulk matrix changed, along with resultant repulsive interactions, which modified the thermodynamic equilibrium. This perturbation increases system immiscibility and leads to the formation of hard domains (second stage). However, hard domain segregation is limited by the nature of hard segments. The low mobility of hard segments stops further segregation and the formation of hard domains become stabilized [20] (third stage).

Fig. 9 illustrates PU-III morphology after different thermo-cycles and *in situ* experiments may be used to explain these results. According to SM tests, thermo-cycle "A" promoted shape recovery; however, the amount of energy introduced into the system was only enough to ensure the first stage of shape recovery. As observed in Fig. 9, the hard domain fraction decreased during cycle-A, but the temperature treatment was not enough to melt crystals, change matrix composition, increase incompatibility and promote new domain formation. Alternatively, cycle-B allowed for the three stages of shape recovery. However, higher values of R_R were not achieved due to the first step of the thermo-cycle, which acted as a stress release treatment and decreased the amount of energy stored in the material during deformation. Therefore, polymeric chains were not able to recover a strongly coiled conformation, leading to lower values of R_R. Thermo-cycle "C" and "E" completed the 3 stages of shape recovery. Thermo-cycle "E" possessed a higher temperature treatment and ensured greater values of R_R due to increased melting of large crystalline fractions.

5. Conclusions

The development of phases during SM cycles applied to poly (ester-urethanes)was successfully monitored using *in situ* SAXS experiments. Recovery and fixation were driven by hydrogen bonding and crystallization. Poor SM results in PU-I may be related to the high degree of phase miscibility, which hinders polymeric chain movement and restricts crystallization during deformation. The SAXS results also showed that the ability to recover shape is related to the rapid re-establishment of specific macromolecular architectures to have their nanostructure rebuilt after the SM cycle. During the recovery stage, soft segment crystallites progressively melted and phase separation increased until a new thermodynamic equilibrium was achieved. The new thermodynamic equilibrium defined the final PU nanostructure.

Acknowledgments

The authors acknowledge financial support from the following institutions: the National Council for Scientific and Technological Development (CNPq), a foundation linked to the Ministry of Science and Technology (MCT) of Brazil, the State of Minas Gerais Research Foundation (FAPEMIG) and the National Synchrotron Light Laboratory (LNLS-Brazil) for use of SAXS beamline facilities.

References

[1] Oertel Günter. Polyurethane handbook. 2nd ed. New York: Hanser Publisher; 1994 (11–45).
[2] Pan H, Chen D. Eur Polym J 2007;43:3766–72.
[3] Chen G, Ma Y, Zheng X, Xu GA, Liu J, Fan J, et al. J Polym Sci B 2007;45 (6):654–60.
[4] Lendlein A, Langer R. Science 2002;296(5573):1673–6.
[5] Gall K, Dunn ML, Liu YP, Stefanic G. Balzar Appl Polym Sci 2004;85(2):290–2.
[6] Gall K, Kreiner P, Turner D, Hulse M. J Micro Sys 2004;13(3):472–83.
[7] Pereira IM, Carvalho S, Pereira MM, Leite MF, Oréfice RL. J Appl Polym Sci 2009;114:254–63.
[8] Bao H, Zhang Z, Ying S. Polymer 1996;37(13):2751–4.
[9] Seymour RW, Cooper RL. Macromolecules 1973;6:48–53.
[10] Kim BK, Lee SY, Xu M. Polymer 1996;37(26):5781–93.
[11] Kim BK, Shin JS, Cho SM, Jeong HM. J Polym Sci Phys 2000;38:2652–7.
[12] Meng Q, Hu JL, Zhu Y, Lu J, Liu Y. Smart Mater Struct 2007;16:1192–7.
[13] Zhu Y, Hu JL, Yeung Kw, Choi Kf, Liu Y, Liem H. Appl Polym Sci 2007;103: 545–56.
[14] Liu Y, Pan C. Eur Polym J 1998;34(5–6):621–4.
[15] Nakamae K, Nishino T, Asaoka S, Sudaryanto. Int J Adhes Adhes 1999;19 (5):345–51.
[16] Pompe G, Pohlers A, Pötschke P, Pionteck J. Polymer 1998;39(21):5147–53.
[17] Chang SL, Yu TL, Huang CC, Chen WC, Linliu K, Lin TL. Polymer 1998;39 (15):3479–89.
[18] Jiang ZY, Tang YJ, Men YF, Enderle HF, Lilge D, Roth SV, et al. Macromolecules 2007;40(20):7263–9.
[19] Wang SH, Zhang Y, Ren WT, Zhang YX, Lin HF. Polym Test 2005;24(6):766–74.
[20] Li Y, Kang WX, Stoffer JO, Chu B. Macromolecules 1994;27(2):612–4.
[21] Pereira IM, Oréfice RL. J Mater Sci 2010;45:511–22.
[22] Miaudet P, Derré A, Maugey M, Zakri C, Piccione PM, Inoubli R, et al. Science 2007;318:1294–6.
[23] Ping P, Wang W, Chen X, Jing X. Biomacromolecules 2005;6(2):587–92.